First publ. in: Journal of Chemical Physics 100 (1994), 2, pp. 995-1010

The development of the 3p and 4p valence band of small aluminum and gallium clusters

Chia-Yen Cha, G. Ganteför, and W. Eberhardt
Institut für Festkörperforschung, Forschungszentrum Jülich, Postfach 1913, 5170 Jülich, Germany

Photoelectron spectra of Al_n^- and Ga_n^- clusters in the size range $n=1$–15 are presented. Using 5.0 and 3.68 eV UV light (KrF excimer and nitrogen laser, respectively), electrons from molecular orbitals corresponding to the 3p and 4p orbitals of the atoms are detached. The spectra reveal a rich fine structure not observed in earlier experiments. The data are compared with the results of quantum chemical calculations. A change in the pattern of the spectra near $n=6$ can be interpreted as a transition from planar to compact 3D structures. The spectrum of Al_{13}^- agrees with the icosahedral structure predicted for this particle. The data do not agree with jellium model predictions. Differences between Al and Ga data can be correlated with the larger binding energy of the Ga 4s band.

I. INTRODUCTION

One main task of cluster research is the closing of the gap between atomic and molecular physics and solid state physics. The electronic structure of small clusters with up to ten or twenty atoms can be described by quantum chemical models[1–10] used in molecular science, and the geometric structure of the cluster can be determined by simulated annealing and total energy minimization. With increasing number of atoms, the detailed geometric and electronic structure becomes more and more complicated and the complexity of these calculations increases with the number of degrees of freedom. On the other hand, the geometric and electronic structures of clusters even with more than 1000 atoms can differ significantly from the solid.[11] Today, high level quantum chemical calculations cannot handle these large systems. In addition, a model including the information of the exact coordinates of each nucleus and the symmetry of each individual electronic orbital might be no longer useful for large clusters.

Any properties requiring a larger particle size for their development, such as metallic properties, cannot be described by quantum chemical methods without adjustable parameters. Therefore, less accurate but simpler models might be more adequate to understand the general behavior of these particles. For metal clusters, a successful approximation is the jellium model[12–14] (JM). This model is used to describe the electronic structure of metal clusters bound by highly delocalized electrons. It is assumed that the electrons are delocalized completely within the boundaries of the whole cluster. The positive atomic cores are smeared out to a uniform positive background charge within the cluster. If the cluster is approximately spherical, the orbitals are degenerate and form shells with defined angular momentum. The predictions of stabilities, ionization potentials, and electron affinities are in reasonable agreement with experiments, if the model includes corrections for aspherical geometries.

Recently we were successful in revealing directly the electronic shell structure in individual clusters using photoelectron spectroscopy on copper cluster anions.[15] The study of coinage metal clusters is a strong support of the validity of the JM for metals with one valence electron per atom. By comparison with Ag spectra,[16] we were additionally able to identify certain features beyond the JM–like shake-up satellites, multiplet splittings, and the *s–d* mixing. Here we extend these measurements to Al and Ga clusters.

Bulk Al is one of the metals that can be well described using a nearly free electron model.[17] However, from different experimental data,[18,19] it is known that small aluminium clusters show deviations from the predictions of the JM. In small clusters, the 3s and 3p bands do not overlap and form separate subsets of electronic states. This lack of overlap of *s* and *p* electrons may be responsible for the deviation from the jellium behavior. With increasing cluster size, a transition into a jellium behavior is expected when the two bands merge.

Here we present a study of Al clusters with a significantly improved resolution and statistics[20] revealing many previously[21–23] undetected features in the spectra. Furthermore, we compare the data to Ga cluster spectra since some of the atomic properties prevail in the formation of the solid state. The comparison of two different elements of the same group of the Periodic Table is very useful for the identification of specific trends in the data. The merging of the *s* and *p* valence bands, in particular, is different for the two metals because the 4s band of Ga is shifted to higher binding energies compared with the Al 3s band.

The data are compared with the results of available calculations. For small clusters ($n<5$), features can be assigned to σ and π molecular orbitals. However, with increasing cluster size, the assignment becomes more difficult, and for clusters with more than $n=13$ atoms, only qualitative differences between the Al and Ga data can be discussed. We hope that this work stimulates the development of new theoretical methods to understand the geometric and electronic structure of these nanoparticles.

II. EXPERIMENTAL SETUP

The experimental setup is described in detail elsewhere.[20] The cluster anions are generated using a pulsed arc cluster ion source (PACIS).[24,25] There are two modifications of the source—one for solid metals and one for metals with low melting points. Al clusters are generated by an electric arc burning between two Al electrodes. The discharge capacitor is 30 μF charged up to 1000 V. The extender (diameter 3 mm) has a length of 5 cm with an 8 cm long conical nozzle. For the generation of clusters of liquid metals, two Mo electrodes are mounted vertically and the liquid is filled into a hole drilled into the tip of the lower electrode. A weak discharge from a small capacitor (0.5 μF) generates sufficient amounts of Ga cluster anions. The same conical nozzle was used as for Al, without an extender.

The internal temperature of the anions is generally unknown. From a line shape analysis of known transitions in photoelectron spectra of Cu_n^- clusters,[20] we estimate the temperature to be comparable to the laser vaporization source [$T_{vib} \approx 165$ K (Ref. 26)]. The mass spectra exhibit impurities (oxides, hydroxides, carbides, etc.), which in some cases interfere with the mass of a bare cluster due to the limited mass resolution. These interfering masses might cause the appearance of additional features in the photoelectron spectra. Impurity features can be identified by a variation of the intensity of the corresponding spectral features compared with the features assigned to the bare cluster, while changing the timing of the detachment laser slightly. However, this method is only applicable if the masses differ. Also, the intensity of the impurity lines may vary with time. We have minimized impurities by using only Al, Mo, and high quality ceramics for the design of the source and high purity He as seeding gas.

The supersonic beam containing helium, neutral, positive, and negative metal clusters passes the skimmer. The anions are accelerated using a high voltage pulse in the acceleration region of a Wiley–McLaren time-of-flight mass spectrometer. The anions are deflected by 90° into the electron spectrometer. The deflection avoids the perturbation of the electron spectrometer by the neutral cluster beam and by the flash of UV light produced during the discharge. A bunch of anions of defined size is irradiated by a UV laser pulse (N_2—3.68 eV, KrF—5.0 eV). For studies of clusters with low electron affinities, visible light from a dye laser is also used. The kinetic energy of the detached electrons is measured using a magnetic bottle type time-of-flight electron spectrometer. The energy resolution depends on the velocity of the electrons and of the anions and varies between 20–200 meV. For KrF, a background due to electrons emitted from surfaces is subtracted from the spectra.

The uncertainty in the absolute binding energy (BE) of the spectra is ± 0.1 eV. The binding energy scale is calibrated using known electron affinities and transitions of various atoms. The relatively large error compared to the energy resolution arises from time dependent changes of the work function of various surfaces within the spectrometer altering the electron kinetic energies slightly. However, the determination of relative peak positions comparing two different clusters is more accurate ($\approx$20–50 meV) due to the short time intervals (≈ 10 min) between those measurements.

III. BASIC MODELS

Two different pictures are used for the interpretation of photoelectron spectra of anions. In the quantum mechanical model, each peak is assigned to a transition from the anion electronic ground state to either the neutral ground state or one of the excited states of the neutral cluster. The detachment process is very fast compared with the vibrational motion, so that the geometry of the cluster remains unchanged. Thus, the spectra contain information about the electronic states of the neutral cluster with the nuclei arranged in the ground state geometry of the anion.

In general, the electron affinity, defined as the binding energy of an additional electron to the neutral particle, cannot be measured using a photodetachment experiment. Only in cases where the vibrational fine structure can be resolved in the spectra and the $0 \leftarrow 0$ transition can be identified is the measurement of the electron affinity possible.[27] Otherwise, only the vertical ionization potential of the anion [VDE (Ref. 28) = "vertical electron detachment energy"] can be determined. The transitions involved and the energetic differences between the electron affinity and the ionization potential of the anion will be discussed in detail (see below).

We assume that the anions are generated in the electronic ground state. The appearance of electronically excited anions in the beam gives rise to additional features in the spectra. In particular, transitions from excited states into the neutral ground state may create new peaks at lower BE than any transition from the cold anions. The lifetime of the excited anion state must be long enough to survive the time of flight to the electron spectrometer. In addition, the excited anion must survive the cooling by the carrier gas. Only in the spectra of the small clusters (see below) there were indications for the existence of electronically excited species in the anion beam.

In laser spectroscopy experiments[29] (e.g., depletion spectroscopy, two photon spectroscopy), only excited states of the neutral species, which can be populated by dipole allowed transitions, can be observed. In photoelectron spectroscopy, the emitted electron carries a certain angular momentum, and a much larger variety of neutral states can be studied because the electron can compensate the angular momentum balance. Photoelectron transitions are governed by two rules (1) the total spin can change only by 1/2, corresponding to the removal of one electron; and (2) the geometry remains unchanged, i.e., each feature exhibits a Franck–Condon profile.

The other picture used in comparison with shell models takes each peak as an indication of electrons detached from a certain one particle orbital within the cluster. The difference between the photon energy and the kinetic energy of the electrons yields directly the binding energy (BE) of each occupied electronic orbital of the anion. This simple model neglects shake-up processes and multiplet

splittings. However, contrary to our previous observations on Cu_n^- and Ag_n^- clusters,[15,16] we found no experimental evidence for shake-up features or multiplet splittings for the Al and Ga data presented here. Using this simple model, assignments of the peaks are given corresponding to single electron orbitals, while in the exact quantum chemical model, peaks in the spectra are assigned to transitions between many body electronic states.

The second picture is also useful if quantum chemical calculations are available only for the neutral ground state. If the binding energies of the corresponding single particle orbitals of the many body ground state are known, peaks in the PE spectra can be assigned to direct emission from these orbitals. Again, this is a crude approximation, since relaxation processes, multiplet splittings, and shake-up processes are neglected. However, most of the available calculations are restricted to the neutral ground states (and sometimes the anion ground state) and thus we use this picture for the assignment of the spectra of the small Al and Ga clusters.

The basic concept of the electronic shell model or jellium model[12-14] (JM) has been discussed above. Any shell model can be applied if a similar symmetry and ordering of shells or orbitals is observed for different species (atoms, nuclei, and clusters) and only the uppermost shell changes while varying the size of the particle (number of protons, baryons, and atoms). Thus, the features in the PE spectra observed for one cluster must be reproduced in the next larger cluster shifted to slightly higher BE due to the increased positive charge of the jellium potential. Using the simple model for the assignment of PE features beyond each shell closing, a new feature should appear at low BE. For nonspherical clusters (ellipsoidal JM[30]), the degeneracies within each shell are partially lifted. Nevertheless, because of spin pairing for every two additional electrons, an additional feature appears. We use these fundamental considerations for testing the validity of a shell model for small Al and Ga clusters.

As mentioned above, features in photoelectron spectra of Cu_n^- clusters[15,16] up to $n=19$ can be assigned to jellium electronic shells of the delocalized s electrons. However, with an increasing number of delocalized electrons per atom (groups II and III of the Periodic Table), the jellium approach is expected to be less valid[31] and we expect substantial deviations from a jellium behavior for small Al clusters. With increasing cluster size, the overlap between the atomic wave functions increases approaching gradually a more jellium-like behavior. The electronic density of states of bulk Al can be well described using a jellium approach.[17]

Upton[31] has suggested corrections of the JM including the modulations introduced by the higher charge of the ionic core. Exact quantum chemical states projected onto jellium wave functions have shown that the orbital filling sequence of the JM is altered for $Al_2^- - Al_6^-$. Introducing corrections which modulate the flat bottom of the jellium potential, the jellium states can be modified towards the quantum chemical exact states. The alteration of the orbital filling sequence depends strongly on the details of the modulation, and an unambigous assignment based on the results of the corrected JM alone is difficult.

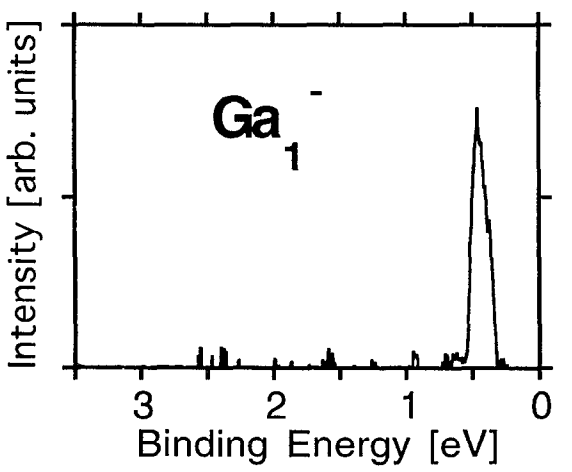

FIG. 1. A photoelectron spectrum of Ga_1^- taken at $h\nu=3.68$ eV. The single feature corresponds to the transition from the anion ground state to the spin–orbit split neutral ground state. The energy resolution is limited to about 0.3 eV due to relatively high kinetic energy of the electrons and the Doppler broadening induced by the velocity of the atoms. The Doppler broadening decreases with increasing cluster mass at constant kinetic energy.

IV. RESULTS

In this section, we present the spectra and discuss experimental details. Our data agree well with previous measurements,[21-23] but due to the improved energy resolution, many more spectral features are resolved.

A. Al_1^-/Ga_1^-

We were not able to record a spectrum of Al_1^-, as the intensity of Al_1^- generated by the source was not sufficient. The electron affinity of Al is 0.441 ± 0.01 eV.[32] For Ga_1^-, the electron affinity is known to be 0.3 ± 0.15 eV.[32] In contrast to Al, the Ga anion is generated by the source at sufficient intensity to record a photoelectron spectrum. Figure 1 displays a PE spectrum of Ga_1^- using 3.68 eV UV light. Only one feature at 0.4 ± 0.2 eV BE is observed. The poor energy resolution for this peak is due to the relatively high kinetic energy of the electrons (3.38 eV), the Doppler broadening caused by the relative high remaining velocity of the monomer, and the doublet structure [spin–orbit splitting $\approx$0.1 eV (Ref. 33)] of this peak. For larger clusters, the Doppler broadening decreases due to the lower velocity corresponding to the same kinetic energy.

B. Al_2^-/Ga_2^-

Figure 2 displays photoelectron spectra of Al_n^- and Ga_n^- clusters with $n=2$–6. Each cluster is studied using two different photon energies $h\nu=3.68$ and 5.0 eV. One reason for changing the photon energy is to lower the kinetic energy of the detached electrons to obtain the maximum energy resolution of the spectrometer. This is demonstrated for peak B located at 3.4 eV BE in the spectrum

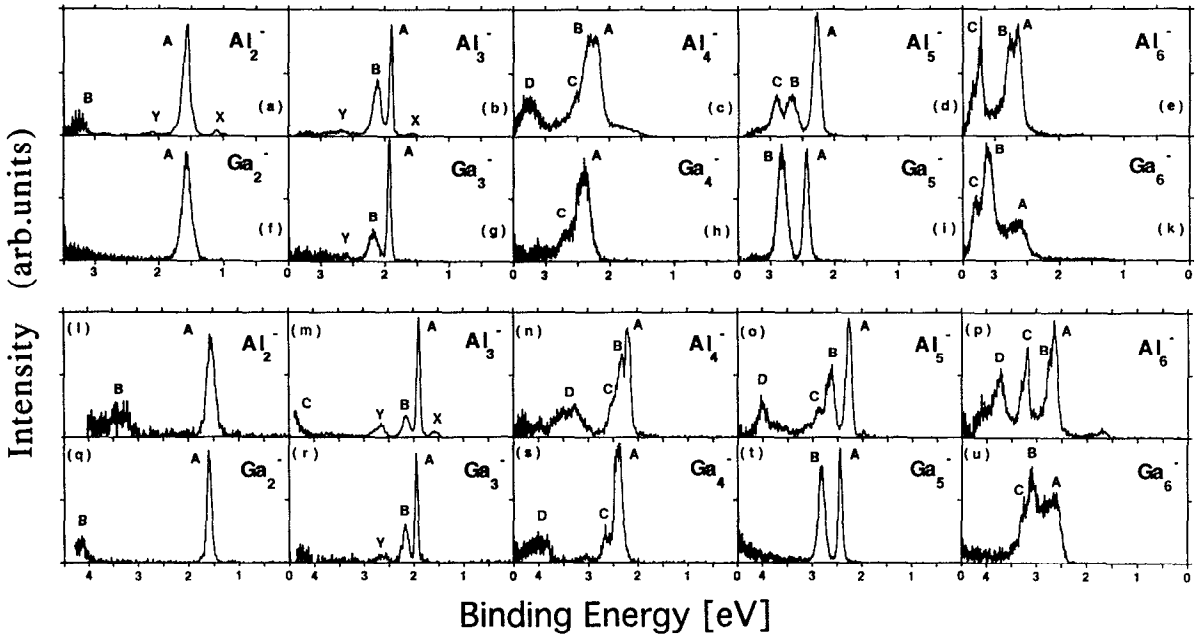

FIG. 2. Photoelectron spectra of (a)–(e) and (l)–(p) Al_n^- and (f)–(k) and (q)–(u) Ga_n^- clusters taken at two different photon energies (a)–(k) $h\nu=3.68$ eV and (l)–(u) $h\nu=5.0$ eV. The energy resolution is improved in the spectra at $h\nu=3.68$ eV due to the lower kinetic energy of the electrons. Using 5.0 eV laser radiation, additional features at higher binding energies can be observed. The minimum pass energy of electrons is 0.5 eV for the 5.0 eV measurements and 0.3 eV for the 3.68 eV measurements depending on slight changes of the surface quality of the spectrometer. The features marked in the figure are discussed in the text. Peaks labeled *A*, *B*, *C*, and *D* are assigned to the bare clusters, while peaks labeled *X* and *Y* are assigned to contaminations of the anion beam like oxides and carbides or to transitions from excited states of the anions. Only the width of feature *A* in the spectra of the trimer is limited by the experimental resolution.

of Al_2^- [Figs. 2(a) and 2(l)]. Using 3.68 eV laser light [Fig. 2(a)], the detached electrons corresponding to feature *B* have a kinetic energy of only about 0.3 eV, and the energy resolution is sufficient to resolve the vibrational structure. Another reason for taking spectra at different photon energies is the photon energy dependence of the detachment cross section for electrons from different orbitals. The variation of the detachment cross section with photon energy depends on the symmetry of the orbital.[34] This results in changes of relative intensities of different features in the spectra. An example is feature *B* in the spectrum of Al_3^- [Figs. 2(b) and 2(m)]. At $h\nu=5.0$ eV [Fig. 2(m)], its intensity relative to feature *A* is lower than in the spectrum taken at 3.68 eV [Fig. 2(b)]. Similar behavior of different peaks suggests similar symmetries and might help in the assignment of the electronic states. Another possible reason for a variation in the photodetachment cross section with photon energy is a resonance with a metastable ion state. This can be studied in detail using tunable light sources.

The spectrum of Al_2^- taken at 3.68 eV photon energy [Fig. 2(a)] exhibits four features. While the prominent peaks *A* and *B* show a stable relative intensity, features *X* and *Y* vary in intensity relative to *A* depending on the expansion conditions of the source. Al_2^- is generated in the source at a very low intensity. The source must be adjusted to low expansion conditions to optimize the dimer intensity. Under these conditions, the cooling of the anions might not be optimal, and impurities show up in the mass spectrum with enhanced intensity. Thus, features *X* and *Y* might be due to impurities. However, it was not possible to record a spectrum at 3.68 eV with zero intensity of feature *X*. Another possible explanation of the appearance of these peaks is the existence of a long lived excited state of Al_2^-. Then feature *X* corresponds to the transition from the excited state of Al_2^- to the neutral ground state. Peak *A* exhibits no vibrational structure even if the spectrum is recorded using green light with 2.33 eV photon energy [Fig. 3(a)]. Feature *B* displays a well-resolved vibrational progression with 55 ± 5 meV spacing [Fig. 2(a)].

The spectrum of Al_2^- taken at $h\nu=5.0$ eV [Fig. 2(l)] exhibits two peaks (*A* and *B*). Features *X* and *Y* might not be observed in this case because of the smaller count rate in this spectrum and because of cross section effects.

The spectrum of Ga_2^- taken at $h\nu=3.68$ eV [Fig. 2(f)] displays a single peak (*A*) located at 1.6 eV BE. At higher photon energy [Fig. 2(q)], a second transition (*B*) at 4.2 eV BE is observed. No clear indication of a vibrational structure could be found for either feature and no additional peaks are observed. This might be due to the different version of the PACIS used for liquid metals. The average anion intensity of Ga clusters is much higher than for Al and nearly no impurities are observed in the mass spectrum. This supports the assignment of features *X* and *Y* to impurities in the spectrum of Al_2^- [Fig. 2(a)]. However, we still cannot exclude the possible assignment of these features to the existence of excited states of Al_2^- because the corresponding excited states of Ga_2^- should be higher in energy and might therefore be less populated in the beam.

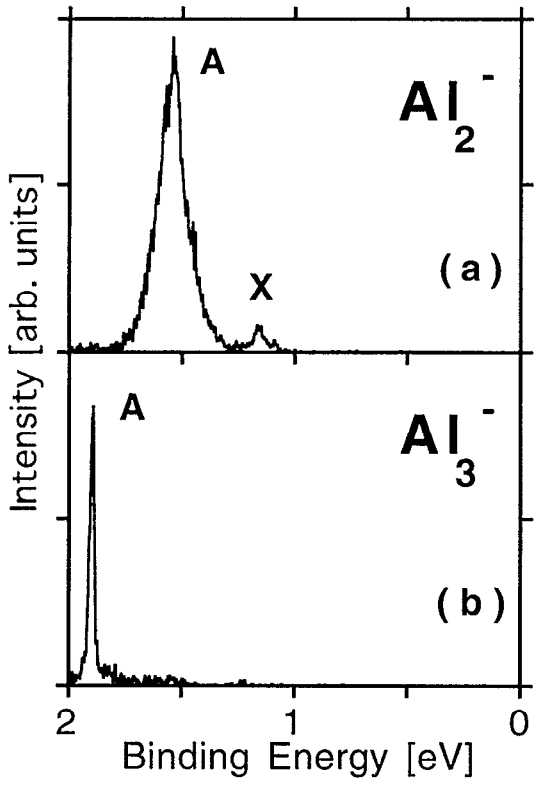

FIG. 3. Photoelectron spectra of Al_2^- and Al_3^- using visible laser light with $h\nu=2.33$ eV. The width of the narrow feature A of Al_3^- corresponds to an experimental resolution of 30 meV.

C. Al_3^-/Ga_3^-

The spectrum of Al_3^- taken at $h\nu=3.68$ eV [Fig. 2(b)] exhibits four features marked A, B, X, and Y. As in the case of Al_2^-, we assign peaks X and Y to impurities or excited anions, and these features will be neglected in the following discussion. The narrow peak at 1.9 eV BE (marked A) has also been studied using visible light with $h\nu=2.33$ eV [Fig. 3(b)]. The observed linewidth is limited by the instrumental resolution to approximately 30 meV. From a zero electron kinetic energy spectroscopy (ZEKES)[35] experiment on Al_3^-, a linewidth of transition A of 15 meV has been determined.[36] Even at the high energy resolution available using ZEKES, no vibrational structure could be resolved. The residual broadening is probably due to the excitation of low energy vibrational modes. The relative intensity of feature B is lower with respect to A in the spectrum taken at $h\nu=5.0$ eV. The spectrum of Al_3^- taken at $h\nu=5.0$ eV [Figs. 2(m) and (4)] possibly exhibits an additional feature C at 4.4 eV BE.

As in the case of the dimers, the Ga_3^- spectra [Figs. 2(g) and 2(r)] are similar to the spectra of Al_3^-. There is a narrow feature (A) at 1.95 eV BE and a broader peak (B) at 2.2 eV BE. In the spectrum taken at $h\nu=5.0$ eV [Figs. 2(r) and 5], no clear indication of a transition at high BE beyond 3 eV is observed. For the weak feature at 2.7 eV BE [Fig. 2(r) marked Y], the same considerations are valid as for feature Y of Al_3^- [Fig. 2(m)]. In Fig. 2(g) (Ga_3^- taken at $h\nu=3.68$ eV), this peak at 2.7 eV BE is close to the noise level. In contrast to Al_3^-, the intensity ratio between the two main features A and B in the spectrum of Ga_3^- does not change drastically with the change of the photon energy.

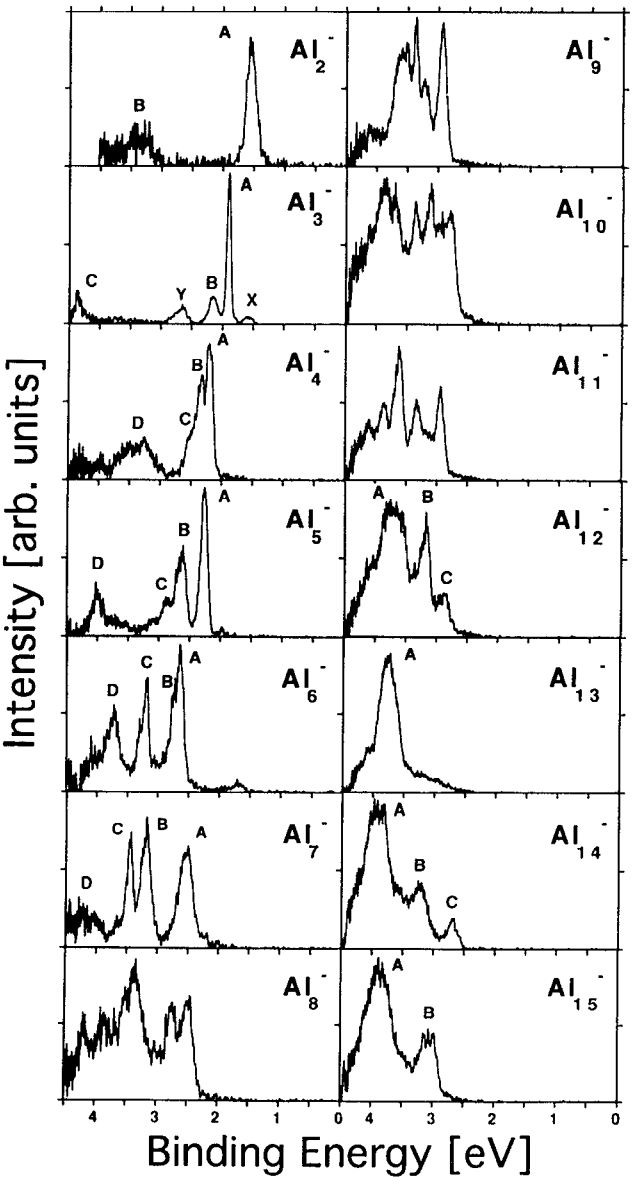

FIG. 4. Photoelectron spectra of Al_n^- clusters with $n=2$–15. The photon energy is 5.0 eV (KrF laser). Most features located at lower BE correspond to photodetachment from $3p$ derived orbitals of Al. The features labeled are discussed in the text.

D. Al_4^-/Ga_4^-

Features with varying relative intensities similar to the peaks labeled X and Y in the spectra of the dimers and trimers are not observed in the photoelectron spectra of Al_n^-/Ga_n^- with $n>3$. Therefore, all observed peaks are assigned to the bare cluster anions. Clusters larger than the trimers are generated by the source at a higher intensity, and the spectra of the larger clusters exhibit an improved signal to noise ratio.

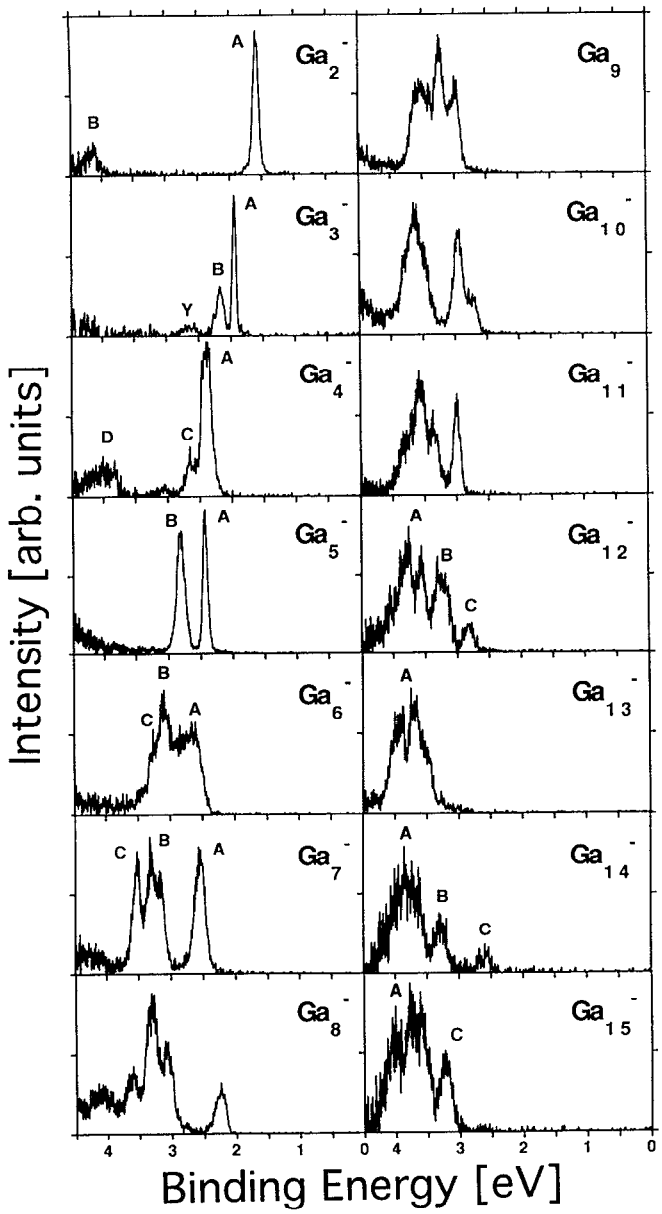

FIG. 5. Photoelectron spectra of Ga_n^- clusters with $n=2$–15. The photon energy is 5.0 eV (KrF laser). All features correspond to photodetachment from 4*p* derived orbitals of Ga. In contrast to Al for Ga_n^- up to $n=11$, a distinct gap between the feature at highest BE and the limit of the experimental range (4.5 eV) is observed, indicating a clear separation of the 4*s* and 4*p* bands.

The spectrum of Al_4^- obtained with $h\nu=5.0$ eV [Figs. 2(n) and 4] displays two prominent broad peaks at 2.5 eV (*A*, *B*, and *C*) and 3.5 eV (*D*) BE. The feature at 2.5 eV BE exhibits a splitting into three components marked *A*, *B*, and *C*. Peak *C* is only visible as a shoulder located at the high BE side of feature *B*. The spectrum of Al_4^- taken at $h\nu=3.68$ eV [Fig. 2(c)] displays the same features with peak *D* cut off at 3.4 eV BE due to the reduced transmission of the spectrometer for low energy electrons. The relative intensities of the three components *A*, *B*, and *C* are altered slightly. At $h\nu=5.0$ eV, peak *B* has a lower intensity with respect to peak *A*.

The three features *A*, *B*, and *C* in Fig. 2(c) ($h\nu=3.68$ eV) are less well resolved than in the measurement at $h\nu=5.0$ eV [Fig. 2(n)]. This behavior is surprising because the energy resolution of the spectrometer is enhanced due to the lower kinetic energy of the electrons corresponding to the same transitions at lower photon energy. In addition, the tail observed at the low BE side of peak *A* has a higher intensity in the 3.68 eV spectrum. These observations might be explained by temperature effects. The source is usually adjusted to a maximum anion signal for each cluster size. Depending on the parameters of the source (seeding gas pressure and timing), the effectivity of the vibrational cooling varies between different measurements. If during the measurement using $h\nu=3.68$ eV the source had run at less effective cooling conditions, the vibrational temperature of the anions would be higher. The peaks would then be broadened and hot band transitions may cause the appearance of an exponential tail at the low BE side of the ground state transition.

The tail at low BE observed for Al_4^- taken at $h\nu=3.68$ eV [Fig. 2(c)] exhibits a width of about 0.5 eV, which corresponds to an extremely high vibrational temperature if the feature is caused by hot band vibrational transitions. Also, the shape deviates from the typical exponential shape of a hot band progression. These tails and a nonstructured smooth photoemission signal at higher BE are observed in several photoelectron spectra of cluster anions (Ag_n^- and Cu_n^-).[15,37] A possible explanation is the appearance of an increasing number of different isomers in the beam at finite vibrational temperatures. The BE of a certain transition in the PE spectrum depends strongly on the geometry (see below). If the spectrum consists of contributions from several isomers different from the ground state geometry, this may cause a nonstructured smooth photoemission signal starting at a BE corresponding to the isomer with the lowest VDE. As long as at lower internal temperature the ground state isomer is still predominant in the beam, a structured photoelectron spectrum can be superimposed to give the featureless sum of spectra of different isomers. These considerations can be verified by calculations using simulated annealing.[1]

We should like to point out here that the difference between the VDE of the isomer with the lowest VDE compared with the VDE of the ground state isomer does not correspond to the difference in total energy of the two isomers. If one single particle orbital is lowered in BE by a change of the geometry, others may be shifted to higher BE. Thus, even if an isomer has a 1 eV lower VDE, the appearance of this isomer in the beam may be due to a much lower thermal excitation energy. This can be demonstrated using the calculations of Al_3 single particle orbitals displayed schematically in Fig. 6. Only the 3*p* derived orbitals are displayed in Fig. 6. The linear isomer of neutral Al_3 (three 3*p* electrons) exhibits a low VDE due to the single electron occupying the $1\pi_u$ orbital. However, the total BE of the linear isomer is relatively high due to the gain of stability corresponding to the increased BE of the two electrons occupying the $2\sigma_u$ orbital (for a detailed discussion s.b.). Thus we are able to explain the appear-

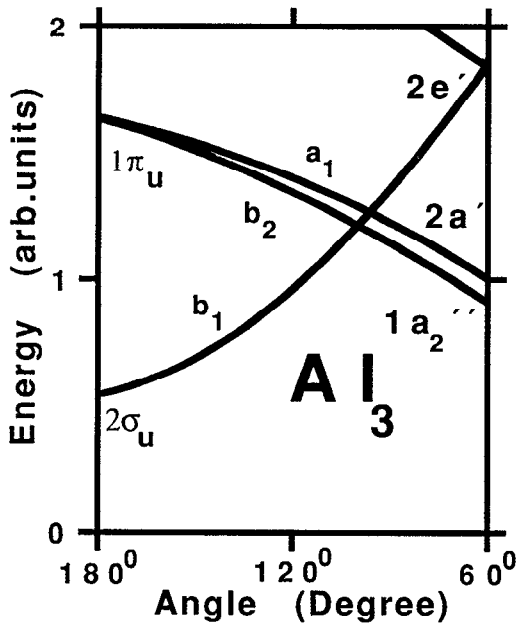

FIG. 6. Mulliken–Walsh diagram of neutral Al_3 taken from Ref. 5. The bond angle of 180° refers to a linear geometry, while 60° corresponds to an equilateral triangle. Only low lying orbitals corresponding to the $3p$ atomic orbitals are shown.

ance of tails exhibiting widths of more than 1 eV in spectra of supersonic cooled anions assuming the existence of low energy isomers. According to quantum chemical calculations,[1–10] the existence of such isomers differing in energy by only a small amount from the ground state is well established.

The spectrum of Ga_4^- obtained with $h\nu=5.0$ eV [Figs. 2(s) and 5] displays two prominent features similar to Al_4^-. However, the feature at lower BE exhibits a substructure corresponding to two components (A and C) only. Peak D is located at about 0.5 eV higher BE in comparison with the corresponding feature D in the spectrum of Al_4^-. At $h\nu=5.0$ eV, the relative intensity of peak C [Fig. 2(s)] has decreased relative to the spectrum at $h\nu=3.68$ eV [Fig. 2(h)].

E. Al_n^-/Ga_n^-, $n>4$

The spectra of Al_5^- and Ga_5^- [Figs. 2(o) and 2(t)] exhibit some similarity to those of the tetramers concerning the number and arrangement of the main features. Again a change of the relative detachment cross section with photon energy is observed for Al_5^- [Feature B of Figs. 2(d) and 2(o)]. The spectra of the larger clusters exhibit an increasing number of peaks according to the increasing number of single electron orbitals (Figs. 4 and 5). The VDE increases gradually and the information obtained from measurements using 3.68 eV photons is limited to the determination of the VDE (s.b.). Thus, a comparison between spectra taken at $h\nu=3.68$ and 5.0 eV seems to be useful only up to $n=6$ (Fig. 2).

Starting from $n=8$, the spectra of Al_n^- exhibit an increasing number of peaks (Fig. 4). For $n=8$, 10, and 11, a strong electron signal is found for all binding energies above the VDE up to the limit of the experimental range. The spectra become simpler again around $n=13$. The spectra of Al_{12}^-–Al_{15}^- are dominated by a broad peak (marked A) at 3.7–4.0 eV BE. Except for Al_{13}^-, this prominent peak is accompanied by one or two additional structures at lower BE (marked B and C). Measurements using ArF laser radiation ($h\nu=6.424$ eV) confirm the observation of this pattern.[38] Up to 6.0 eV BE, no further peaks are found beyond the limit of the experimental range of Fig. 4 (=4.5 eV BE). Therefore, within the range of binding energies corresponding to the Al $3p$ band, the spectra of Al_{12}^-–Al_{15}^- are dominated by a single broad peak accompanied by smaller structures except for Al_{13}^-, where only the main feature is observed.

The pattern observed in the spectra of the larger Ga_n^- clusters is slightly different (Fig. 5). In the size range $n=6$–11, the Ga_n^- spectra exhibit qualitative differences from the corresponding Al_n^- data. The spectra of Ga_8^-, Ga_{10}^-, and Ga_{11}^- are less complex than the Al data and the bandwidth of the range of observed transitions is smaller. An exception to this behavior is Ga_7^-, which resembles the spectrum of Al_7^-. The spectra of Ga_n^- do not exhibit the striking pattern observed for the Al clusters at $n=12$–15. In contrast to Al_{13}^-, the spectrum of Ga_{13}^- displays a double peak, indicating a lower symmetry compared with Al_{13}^-. However, the bandwidth of the group of features observed within our experimental range exhibits a local minimum for Ga_{13}^- (e.g., compared with Ga_{12}^- and Ga_{14}^-), indicating a higher degree of degeneracy of the electronic states.

By comparison with the Al spectra, some indications for the existence of the pattern observed in the size range $n=12$–15 for Al can be found in the Ga spectra also. If one assumes that for Ga clusters the corresponding feature exhibits a split structure, a pattern similar to the Al spectra can be identified for Ga_{12}^-–Ga_{15}^-. The feature (Fig. 5, marked A) corresponding to the main peak in the Al spectra exhibits a splitting into two (Ga_{12}^- and Ga_{13}^-) or even three peaks (Ga_{15}^-). Then the analogous assignment can be made for Ga as for Al.

From the considerations discussed above, the spectra of the cluster anions can be divided into three size regimes:

1. $n=2$–7

The spectra are dominated by one to three features grouped into a narrow BE range, which increases with increasing cluster size. The spectra of Al and Ga clusters are very similar except for the features at higher BEs. A pronounced dependence of the cross section on the photon energy is observed for certain features.

2. $n=8$–11

The spectra of the Al clusters exhibit an increasing complexity with a high density of states covering a broad range of binding energies. There are qualitative differences between the Al and Ga spectra, with the Ga spectra being less complex and exhibiting a smaller bandwidth of the $4p$ band.

3. $n=12$–15

The spectra of Al clusters are dominated by a single broad feature which is accompanied by one or two smaller peaks. For Al_{13}^-, only the single feature is observed. The spectra of the Ga cluster exhibit the same pattern, if we assume for Ga a splitting of the broad feature observed for Al into two or three components.

In the following section, we discuss the data in terms of different models and try to find explanations for the trends and patterns revealed by the photoelectron spectra.

V. DISCUSSION

We compare the data to the predictions of two different theoretical approaches for the electronic and geometric structure of metal clusters. The jellium model is very successful for the explanation of the electronic shell structure and the oblate–prolate deformation observed for monovalent clusters.[14,16] A more elaborate approach is based on quantum chemical calculations,[1–10] with the electronic ground state energy being calculated while varying the geometric structure. The global minimum of the total energy corresponds to the ground state structure.

A. The jellium model

The jellium model (JM) is very successful interpreting the photoelectron data of monovalent metal clusters (e.g., Cu_n^- and Na_n^-).[16,39] The predicted shell closings at 8,18,20,... electrons are clearly observed, manifesting themselves in various properties of the clusters.[14] Those clusters exhibit a pronounced even–odd alternation, which can be explained by the JM assuming ellipsoidal distortions of the clusters.[30]

Clusters of group III elements (B, Al, Ga, In, and Tl) do not exhibit marked shell closings because each atom adds three electrons to the cluster. Only for a few cases, the number of electrons matches a shell closing. This is the case for Al_{13}^- and Ga_{13}^- with 40 valence electrons. The photoelectron spectrum of Al_{13}^- (Fig. 4) exhibits a relatively high VDE (s.b.) and only a single broad feature within the energy range measured. The spectrum of Ga_{13}^- (Fig. 5) is similar [except for the fine structure of the single peak (s.b.)]. This observation of a pronounced shell closing corresponding to 40 electrons and the free electron behavior of bulk Al (Ref. 17) justify an attempt to apply the ellisoidal JM interpreting the spectra.

However, the spectra of the small clusters (Al_n^-, $n<12$) do not reflect the behavior predicted by a shell model. As an example, we compare the spectra of Al_4^- and Al_5^- with the predictions of the JM. The JM configuration of the 13 electron cluster Al_4^- is $1s^2 1p^6 1d^5$. According to the JM, Al_5^- should possess eight electrons occupying the $1d$ shell. If the cluster is not spherical, four features corresponding to the occupied $1d$ subshells should appear in the spectrum of Al_5^- at the lowest BE. This behavior is indeed observed for Cu_{15}^-.[15] However, the spectrum of Al_5^- exhibits the same number of peaks as Al_4^- (Fig. 2) located at about the same BE, even though Al_5^- has three additional valence electrons.

From molecular orbital considerations, the observation is easy to understand—the three features *A*, *B*, and *C* at low BE in the spectra of Al_4^- and Al_5^- [Figs. 2(n) and 2(o)] are assigned to photodetachment from σ and π orbitals of the $3p$ band. Al_4^- has five and Al_5^- has six electrons occupying $3p$ derived orbitals. Thus, due to the spin degeneracy, no additional feature is expected to appear in the spectrum of Al_5^-. The other two additional electrons of Al_5^- occupy an additional $3s$ derived molecular orbital at high BE beyond the present range of our experiment. From these considerations, we assume that as long as the two bands $3p$ and $3s$ do not merge, the JM is unlikely to be valid.

The two bands merge into the bulk valence band, so that hybridization of the bands should be observable at some cluster size. The exact size at which this occurs is still a matter of discussion in the literature. From electrostatic polarizability measurements,[18] a nonjellium/jellium transition is found for Al_n at $n\approx 40$. The photoelectron data of Taylor *et al.*[21] suggest a mixing starting at $n\approx 30$. From the discussion of our spectra based on quantum chemical calculations (see below), we find indications for an onset of hybridization between antibonding $3s$ and bonding $3p$ orbitals for $n>8$. Indeed, starting from $n=12$, the photoelectron spectra of the Al clusters exhibit a much simplified pattern which might correspond to the development of a shell structure. However, there is evidence for the existence of a pronounced gap between the $3s$ and $3p$ bands even for $n=20$.[21,38] Further measurements using higher photon energy extended to larger cluster sizes are needed to test the validity of the JM and to establish the cluster size for which the two bands start to overlap.

One approach[2,31] introduces a modulation of the flat jellium potential which can be treated as a perturbation. This modulation corresponds to the relatively high charge of the ionic cores. The perturbation causes a reordering of the single particle states that are degenerate in angular momentum eigenstates if the perturbation is zero. Including this correction, the JM should be able to describe the separation of the single particle states into the $3s$ and $3p$ bands in small Al clusters. With increasing cluster size, the two bands merge corresponding to a decrease of the perturbation. However, the results of this perturbated JM depend on the exact positions of the ionic cores within the cluster. Due to the lack of detailed calculations based on this approach, we cannot compare our data with this model.

B. Quantum chemical calculations

A clear assignment of the features is only possible by comparison with quantitative calculations (see, e.g., Ref. 9). Our discussions here, however, will be limited to qualitative comparisons. Nevertheless, a simple picture of the changes in the electronic and geometric structures in these small Al and Ga clusters will emerge from these considerations.

1. Al_1^-/Ga_1^-

Al_1^- could not be generated using the PACIS, therefore only the spectrum of Ga_1^- could be obtained as shown in Fig. 1. The electron affinity of Ga_1^- extracted from Fig. 1 is 0.45 ± 0.2 eV. The large error is due to the relatively high kinetic energy of the electrons. The value agrees within the limits of uncertainty with the literature value (0.3 ± 0.15 eV).[32]

Both neutral atoms have two s and a single p electron in the outer $3(4)s$ and $3(4)p$ shells (values given in parentheses correspond to Ga). Therefore, the neutral ground state is in both cases a doublet $^2P_{1/2,3/2}$. The spin–orbit splitting of the Ga ground state is 0.10 eV (Ref. 33) and cannot be resolved in our spectrum. The first excited state of the neutral Ga is a $4p \rightarrow 5s$ excitation into a ^2S state at 3.07 eV with respect to the neutral ground state.[33] This would correspond to a shake-up feature at 3.37 eV BE and is not observable in our spectrum. Electrons from the $3(4)s$ orbitals of the atoms cannot be detached with even the highest applied photon energy (5.0 eV) in this experiment.

The first excited state (^2S) corresponding to a $3s \rightarrow 3p$ exitation in neutral Al is at 6.416 eV excitation energy.[33] For Ga, the same excitation requires 7.70 eV,[33] i.e., a feature corresponding to emission from the $4s$ orbital in Ga_1^- should appear first at 7.73 eV BE, far out of the present range of our experiment. Detachment of a $3(4)s$ electron of Al_1^- (Ga_1^-) corresponds to a transition into excited states of the neutral (occupation sp^2) with two electrons in the $3(4)p$ orbital. The two electrons can combine to different spin and angular momentum states and would show up as a multiplet in the PES.

Important for the understanding of systematic shifts observed in the cluster PES is the difference of the $3s$–$4s$ BEs between Al and Ga.[10] The BEs of the $3(4)p$ orbitals of the two different atoms are similar which can be seen from a comparison of the electron affinities of the atoms—about 0.441 eV (Ref. 32) for Al_1^- and 0.3 eV (Ref. 32) for Ga_1^-. Applying the simple model for interpretation of the PES discussed above, we assume that the difference between the photon energy and kinetic energy of electrons detached from the corresponding orbital is equal to the BE of the orbital. Especially, the BE of the outermost orbital of the anion is equal to the electron affinity of the cluster. The $3s$ orbital of Al_1^- has a BE of 6.42 eV, while the corresponding $4s$ orbital in Ga_1^- is shifted by 1.31 eV towards higher BE ($=7.73$ eV). This qualitative difference enables us to identify peaks belonging to the $3(4)s$ derived electronic states in PES of the cluster if the s and p bands are well separated.

2. Al_2^-/Ga_2^-

In the Al dimer anion, the $3s$ orbitals of the atoms combine to σ and σ^* orbitals filled with four electrons. Because bonding and antibonding orbitals are both filled, the $3s$ states contribute only weakly to the bonding. The $3p$ orbitals combine to two σ and four π orbitals. For the neutral Al dimer, it is known that the $^3\Pi_u(\sigma_g\pi_u)$ and $^3\Sigma_g^-(\pi_u^2)$ states are nearly degenerate, i.e., relatively little energy is required for $\sigma_g \rightarrow \pi_u$ transfers.[9] Al_2^- has three electrons in the $3p$ derived orbital which give rise to doublet or quartet states. The anion ground state is the quartet state corresponding to the three electrons distributed into the three bonding orbitals ($\sigma_g\pi_u^2$) with parallel spins ($^4\Sigma_g^-$).[9] Detachment of one of these electrons corresponds to a transition into one of the nearly degenerate ground states of the neutral dimer.[9] The neutral dimer has two $3p$ electrons, which can combine to singlet or triplet states. Only the triplet states can be populated by photodetachment from a quartet state. According to recent experiments,[40] the ground state of the neutral dimer is $^3\Pi_u(\sigma_g\pi_u)$, with the $^3\Sigma_g^-(\pi_u^2)$ state less than 25 meV higher in energy. We assign peak A [Figs. 2(a), 2(1), and 3(a)] to the transition from the anion quartet state to the two triplet states of the neutral. Peak A exhibits a width of approximately 180 meV [Fig. 3(a)]. The Franck–Condon broadening due to the removal of one bonding electron is too large to enable us to resolve the different triplet states. In addition, the two nearly degenerate states may cause a complex vibrational structure. This might explain why we were not successful in resolving any vibrational structure for feature A [Fig. 3(a)]. From the spectrum, we determine the VDE to be 1.6 ± 0.1 eV.

Feature B in the spectrum of Al_2^- at 3.3 eV BE corresponds to a transition into an excited state of the neutral dimer. In the single particle picture, transitions into excited states correspond to the detachment of an electron from deeper orbitals. The $3s$ level of the Al atom is located at 6.42 eV higher BE with respect to the $3p$ orbital. In the dimer, the corresponding σ orbital splits into a bonding and an antibonding orbital. Removal of an electron from the antibonding σ^* will increase the bond strength by enhancing the bond order formally by 0.5. The detachment of an electron from the σ^* orbital of Al_2^- corresponds to a transition into an excited state of the neutral with one electron promoted from the antibonding $3s$ σ^* orbital into a bonding $3p$ π orbital. Thus, the bond order is increased by 1 compared with the neutral ground state. The relatively high vibrational frequency (55 ± 5 meV$\approx 450 \pm 40$ cm^{-1}) experimentally observed for peak B [Fig. 2(a)], which is much higher than the ground state frequencies of both the anion[9,10] (≈ 330 cm^{-1}) and the neutral[9,10] dimer (≈ 350 cm^{-1}) is in agreement with these considerations. In addition, these considerations agree well with the prediction[9] of a vibrational frequency of 435 cm^{-1} for the $^5\Sigma_u^-(\sigma_g^2\sigma_u\sigma_g\pi_u^2)$ state of the neutral dimer. Therefore, we assign feature B to the detachment of an electron from the antibonding σ^* orbital of the $3s$ band corresponding to a transition from the anion ground state into the $^5\Sigma_u^-$ excited state of the neutral. The equilibrium bond length changes due to the detachment which explains the broad Franck–Condon progression observed for this feature.

At low kinetic energies (as in our case), the single particle picture might fail and shake-up processes involving more than one electron lead to transitions into a larger variety of states. One possible shake-up process is the simultaneous excitation of one of the electrons occupying the

bonding $3p$ orbitals (σ,π) into an antibonding orbital (σ^*,π^*). However, the relatively high vibrational frequency observed experimentally does not agree with this assumption of a transition into an antibonding orbital. The strength of the bonding in the neutral dimer would be lowered, corresponding to a lower vibrational frequency compared with the ground state.

Ga_2^- should exhibit similar transitions in the spectrum. Feature *A* [Figs. 2(f) and 2(q)] is assigned to the transition into the two nonresolved triplet ground states of neutral Ga_2. The VDE is 1.6 ± 0.1 eV and similar to Al_2^-. In contrast to the corresponding peak *B* of Al_2^- [Fig. 2(a)], feature *B* displays no resolved vibrational structure. The experimental energy resolution for electrons corresponding to feature *B* is about 35 meV, which therefore is an upper limit of the vibrational frequency of this excited state of the neutral dimer. Feature *B* is located at about 1 eV higher BE than the corresponding peak of Al_2^-. The BE difference between $3(4)s$ and $3(4)p$ for the atoms[33] is increased by 1.28 eV for Ga. If we assume similar differences of the BEs for the $3s$ derived states in the clusters, this is in reasonable agreement with the observed binding energy difference between feature *B* of Ga_2^- and feature *B* of Al_2^-. It is strong support of the assignment of these two peaks to detachment from the antibonding $3(4)s$ σ^* orbital. The assignment also agrees with the results of calculations[9] on Ga_2^- and neutral Ga_2. For the larger clusters, the difference in BE for $3s(4s)$ derived orbitals between Al and Ga spectra will be used as an indication of the assignment of certain features as parts of the $3s$ band.

3. Al_3^-/Ga_3^-

There are various calculations and experiments concerning the nature of the neutral ground state of Al_3, the low lying excited electronic states, and the geometry (see, e.g., Ref. 9 and references therein). The main facts can be explained using Fig. 6, which has been taken from Ref. 5. In this schematic Walsh–Mulliken diagram, the BEs of the single particle molecular orbitals corresponding to the $3p$ levels of the three atoms are plotted as a function of the bond angle in the triangular molecule (180°=linear). The influence of the $3s$ electrons has been neglected.

According to Fig. 6, the equilibrium geometry of the cluster changes depending on the number of $3p$ electrons (Al_3^+, Al_3, and Al_3^-). The change in total energy is reflected by the change in the single particle energies of the valence electrons. Accordingly, the ground state of Al_3^+ is linear with both $3p$ electrons occupying the $2\sigma_u$ orbital which is the minimum energy possible for an occupation of two electrons in Fig. 6. On the other hand, both neutral Al_3 and Al_3^- have ground states with equilateral triangular geometry. Two electrons occupy the $1a_2''$ orbital and one or two occupy the $2a'$ orbital, respectively. The ground state of the anion is a singlet $^1A_1$ state ($1a_2''^2,2a'^2$). The ground state of the neutral Al_3 is $^2A_1$ with an occupation of $1a_2''^2 2a'$. At about 0.22 eV [0.32 eV (Ref. 9)] higher energy, the existence of a $^2B_2$ state with the occupation $1a_2''2a'^2$ is predicted. Quartet states are neglected in this discussion due to the photodetachment selection rules corresponding to detachment from a singlet state. It should be mentioned that the results of the calculations vary, depending on the methods and levels of sophistication, with respect to the order of the levels and the dependence of the BEs on the geometry. However, concerning the neutral and anion ground states, the qualitative agreement with the results displayed in Fig. 6 is remarkable.

Peaks *A* and *B* (0.21 ± 0.03 eV splitting) in the spectrum of Al_3^- are assigned to transitions from the $^1A_1$ state into the $^2A_1$ state and the $^2B_2$ [Refs. 9 and 10 ($^2B_1$)] state of Al_3, respectively [0.22 (Ref. 5) or 0.32 eV (Refs. 9 and 10) predicted splitting]. The difference in BE between the two features coincides well with the calculated difference between the two lowest doublet states of the trimer. Thus, the two peaks correspond to detachment of an electron either from the $1a_2''$ or the $2a'$ orbital. The $1a_2''$ orbital is a π bonding orbital normal to the molecular plane. The $2a'$ orbital has dominant σ character. Analogous to the dimer, the spectrum of $3p$ derived features consists of two close lying features with σ and π symmetries. Because both states of the neutral trimer exhibit about the same geometry as the anion (equilateral triangle), both features should be very narrow if the bond lengths are not altered. However, only the detachment of an electron from the outermost orbital ($2a'$ according to Ref. 5) does not influence the geometry strongly {feature *A* [Fig. 3(b)]} Peak *B* [Fig. 2(b)] exhibits a broadening due to a substantial geometry change.

Feature *C* in the spectrum of Al_3^- taken at $h\nu=5.0$ [Fig. 2(m)] is assigned to detachment from the antibonding orbital of the $3s$ band. This assignment is supported by the spectrum of Ga_3^- [Fig. 2(r)]. It exhibits nearly the same features as the spectrum of Al_3^- with the same assignments. However, we expect that all orbitals derived from the $4s$ band exhibit an about 1 eV higher BE. Thus, the feature corresponding to *C* of Al_3^- is missing in Fig. 2(r) because its BE is probably beyond the present range of our experiment.

The relative intensity of peak *B* in the spectrum of Al_3^- varies with photon energy. At higher photon energy, the intensity ratio between peak *B* and the dominant feature *A* decreases. This can be explained by a cross section effect. Peak *B* is assigned to a transition from the anion ground state $^1A_1$ to the first excited state $^2B_1$ of neutral Al_3. The electron is detached from a π-like orbital. For atoms, the detachment cross section of electrons occupying *p* orbitals rises to a maximum within a few millielectron volts above threshold, while the cross section for detachment from *s* and *d* orbitals increases more gradually with photon energy.[34] Thus, a few electron volts above threshold, the relative intensities of features corresponding to detachment from *s* and *d* orbitals is still increasing with photon energy, while the cross section for detachment from *p* orbitals remains about constant. This observed variation of the relative cross sections of the two features corresponding to detachment from the $1a_2''$ and $2a'$ orbitals is in agreement with their supposedly dominant *p* and *s* character.

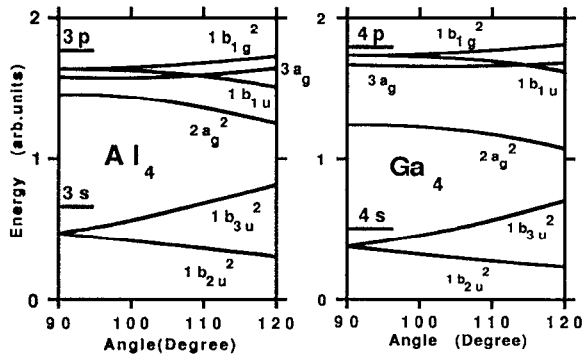

FIG. 7. A comparison of the single particle orbitals of the valence band of Al_4 and Ga_4 assuming a planar geometry taken from Ref. 3. The bonding 3*s* orbital is not shown in the figure. The bond angle of 90° corresponds to a square. With increasing angle, the square is deformed into a rhombus. All orbitals belonging to the 4*s* band of Ga_4 are shifted to higher BE compared with Al_4. According to these calculations, the ground state of Al_4 is rhombic (angle=110°), while Ga_4 is a perfect square. The orbitals shown are occupied by 11 electrons in the case of the anions.

The cross section variation is less pronounced for Ga. The observed changes of relative peak intensities are small for Ga_3^-–Ga_5^- in comparison with the corresponding Al cluster data. The two atoms Al and Ga differ by the size and number of nodes of the radial wave functions of the atomic valence orbitals. The photon energy dependence of detachment cross sections might therefore be shifted in energy even for orbitals of the same symmetry. If the jellium model would be a valid description of the cluster, no large differences of the dependence of the cross sections on the photon energy are expected. Contrary to the atomic wave functions, the jellium wave functions have the same node structure for Al and Ga clusters. For a detailed analysis, a more elaborate experimental study of the photon energy dependence is necessary.

4. Al_4^-/Ga_4^-

Figure 7 displays a Mulliken–Walsh diagram of the single particle orbitals of the neutral tetramers[3] of Al and Ga. Most calculations[1–3,6–8,10] predict a planar geometry for Al_4. The orbital energies (Fig. 7) are displayed as a function of the angle corresponding to the transition between a square and a rhombic geometry. There are four orbitals originating from combinations of the 3*s* wave functions of the atoms (the lowest 3*s* derived orbital is not shown in Fig. 7) and three of the low lying orbitals corresponding to the 3*p* orbitals of the atoms. For the neutral cluster, the 3*s* orbitals are fully occupied, while the 3*p* derived orbitals are occupied by four electrons. As in the case of the dimer, the near degeneracy of the lowest 3*p* orbitals gives rise to several low lying electronic states with different occupations and spin multiplicities. The existence of several low energy isomers with singlet or triplet ground states has to be considered.[10] With increasing cluster size, the electron–electron interaction[10,16] decreases for delocalized valence electrons and the ground states of the clusters are either singlet or doublet states according to an even or odd total number of electrons in the cluster. According to calculations, Al_n clusters with $n>5$ have ground states with minimum spin multiplicity.[10]

We propose a tentative assignment of the data using the results on the neutral species shown in Fig. 7. We assume the additional electron occupies the outermost orbital resulting in a doublet state. We neglect any changes in electronic and geometric structures induced by the additional charge. This approximation is partially supported by the photoelectron spectra because the features do not exhibit a strong vibrational broadening, indicating a small geometry change due to neutralization. We also neglect shake-up processes. The cross section for shake-up processes depends on the electron–electron interaction and is expected to decrease with increasing cluster size for delocalized electrons. However, the valence electron density is higher in Al clusters compared with, e.g., Cu (Ref. 16) and shake-up processes might therefore be more likely. Thus, a comparison of the photoelectron spectra with the results of the calculations displayed in Fig. 7 can only be tentative.

In terms of the simplest model used for the assignment of peaks in photoelectron spectra, each occupied orbital corresponds to a feature in the spectrum. With the maximum photon energy used in our experiment ($h\nu=5$ eV), detachment from the uppermost antibonding 3*s* orbital ($2a_g^2$) and the three 3*p* derived orbitals ($1b_{1u}$, $3a_g$, and $1b_{1g}$) can be observed. According to Fig. 7, the three 3*p* derived orbitals are close in energy and the level ordering depends strongly on the exact geometry. For a square geometry, the orbital at lowest BE is twofold degenerate and corresponds to π bonding ($1a_{1u}$ and $1b_{1g}$). The orbital corresponding to σ bonding ($3a_g$) is located very close at somewhat higher BE.

From these considerations, we expect the appearance of three peaks at low BE corresponding to the 3*p* orbitals and one peak at higher BE corresponding to the antibonding 3*s* orbital. The 3*s* feature should appear at about 1 eV higher BE for Ga_4^- and should exhibit a relatively large vibrational broadening corresponding to its antibonding character. This is in suprisingly good agreement with the experimental observations [Figs. 2(n) and 2(s)]. Therefore, we assign the three features *A*, *B*, and *C* in the spectrum of Al_4^- [Fig. 2(n)] to transitions corresponding to detachment from the three 3*p* derived orbitals ($1b_{1u}$, $3a_g$, and $1b_{1g}$) displayed in Fig. 7. Peak *D* in the spectrum of Al_4^- taken at $h\nu=5.0$ eV is assigned to photodetachment from the $3a_g$ orbital. The assignments are similar in the case of Ga_4^-. Due to a slightly different geometry of the anions peak *A* and *B* observed as a double feature for Al_4^- are degenerate in the spectrum of Ga_4^- {peak *A* [Fig. 2(s)]}.

Upon changing the excitation energy for Al_3^-, we observe an increase of the relative intensity for a feature assigned to emission from a σ orbital. In the case of Al_4^-, peak *A* exhibits a similar increase relative to *B* and *C* [Figs. 2(c) and 2(n)]. This might suggest the assignment of fea-

ture A to the σ orbital ($3a_g$). However, the experimental data are not sufficient for a detailed analysis of the cross section dependence on the photon energy. A possible extension is the study of the cross sections close to the thresholds as demonstrated[41] for Si_2^-.

5. Al_5^-/Ga_5^-

To our knowledge, there are no data published on the single particle orbital BEs for the valence band orbitals of Al and Ga clusters larger than $n=4$. There are several calculations on the ground state properties and some low lying excited electronic states for clusters up to ten atoms (see, e.g., Ref. 9 and references therein). However, with increasing cluster size, the comparison of the PE data with calculations of energies of excited states becomes difficult. The number of electronic states depends on the number of valence electrons. The interpretation of the spectra as detachment from certain molecular orbitals reduces the number of states accessible by detachment (see above). For the larger clusters, we can only discuss certain tendencies in the spectra.

For Al_n, a transition from planar to 3D structures is predicted[1] to occur at $n=5$. For Al_5, two nearly degenerate isomers[1] have been calculated with a planar and a three dimensional structure. There are some similarities between the spectrum of Al_5^- [Fig. 2(o)] and the spectrum of Al_4^- [Fig. 2(n)]. In both spectra, three peaks can be assigned to the $3p$ band (marked A, B, and C). The number of electrons occupying $3p$ derived orbitals increases from Al_4^- to Al_5^- from 5 to 6. Thus, if the spectra are a direct picture of the occupied orbitals and the symmetry of the orbitals is similar, no large change in the spectra is expected. A half-filled $3p$ derived orbital of Al_4^- is occupied by two electrons in Al_5^-. Feature D at 4.4 eV BE in Fig. 2(o) is assigned to the antibonding orbital of the $3s$ band, as in the case of the tetramer. A corresponding peak is not observed for Ga_5^- [Fig. 2(t)] according to the about 1 eV higher BE of the $4s$ derived features in Ga. The corresponding transition would be located at 5.5 eV BE, well beyond the present range of our experiment.

The spectrum of Al_4^- is in reasonable agreement with the assumption of a planar geometry of both the anion and the neutral. From the similarity of the photoelectron spectra of Al_4^- and Al_5^-, we tentatively infer a similarity of the electronic and geometric structures. According to this similarity, the ground state geometry of Al_5^- might be planar or close to planar (buckled). Features A, B, and C can be tentatively assigned to three occupied bonding σ and π orbitals of the $3p$ band. Accordingly, the electronic ground state of Al_5^- would be a singlet state.

The spectrum of Ga_5^- [Fig. 2(t)] exhibits an analogous similarity to the spectrum of Ga_4^-. Two features (A) and (B) are observed at low BEs and are assigned to $4p$ derived states. As in the case of the tetramers, two peaks observed for Al_5^- [Fig. 2(o), marked B and C] are degenerate in the Ga_5^- spectrum [Fig. 2(t) marked B]. Therefore, the geometry of Ga_5^- seems to be only slightly different from Al_5^-.

6. Al_n^-/Ga_n^-, $n=6$ and 7

In the spectrum of Al_6^- [Figs. 2(e), 2(p) and 4], we assign features A, B, and C to emission from $3p$ derived orbitals and peak D analogous to the spectrum of Al_5^- to emission from the highest antibonding orbital of the $3s$ band. This assignment is supported by the spectrum of Ga_6^- [Figs. 2(k), 2(u) and 5], which exhibits no feature in the binding energy range corresponding to peak D of Al_5^-. This is expected for a feature corresponding to emission from the $3s/4s$ band as discussed above. However, the spectrum of Ga_6^- differs relatively strongly from the spectrum of Al_6^- and therefore the assignment of feature D of Al_6^- is less certain.

In contrast to the six atom clusters and all larger clusters, the spectra of Al_7^- and Ga_7^- (Figs. 4 and 5) are again very similar, indicating a similar electronic and geometric structure. Therefore, we assign the three prominent features (A, B, and C) of Al_7^- to $3p$ emission and the corresponding peaks of Ga_7^- to $4p$ emission. The weak peak D in the spectrum of Al_7^- might be assigned to emission from the $3s$ band, but for a definite assignment, measurements at higher photon energy[38] would be necessary.

For both Al_6^- and Al_7^-, there is still a similarity in the structure of the photoelectron spectra comparable with Al_4^- and Al_5^- (Fig. 4). There are three main features assigned to photodetachment from $3p$ derived states and, located at slightly higher BE, a single feature assigned to $3s$ emission. If the assignment is correct, the three features corresponding to $3p$ photoemission correspond to four partially degenerate molecular orbitals occupied by seven or eight electrons. The $3p$ bandwidth increases smoothly with increasing cluster size from Al_2^- to Al_7^-.

For the neutral Al clusters, a transition from planar structures to 3D geometries starting from $n=5$ is predicted.[1,10] The similarity of the spectra of Al_6^- and Al_7^- might be an indication for a planar or buckled structure of these particles in contrast to the larger clusters that no longer exhibit a similarity to the photoelectron spectra of Al_3^- and Al_4^-.

7. Al_n^-/Ga_n^-, $n=8$–11

Starting from Al_8^- (Fig. 4), the spectra exhibit a different pattern compared with the spectra of the smaller Al clusters. A large number of transitions is observed for Al_8^-–Al_{11}^- which are partially overlapping. Based on the experimental data available, it is very difficult to distinguish between $3s$ and $3p$ derived electronic states. The spectra of the Ga_n^- clusters of the same size exhibit a pronounced gap corresponding to a low photodetachment signal in the BE range between 4.0 eV and the cutoff of the spectrum at 4.5 eV. We assign this gap to the upper part of the $4s$–$4p$ band gap expected for small Ga clusters. Therefore, for Ga clusters of that size, the two valence bands are still well separated. No such pronounced gap is observed for Al_8^-, Al_{10}^-, and Al_{11}^- (Fig. 4). If the high density of states observed in the spectra of these Al clusters is assigned to emission from the $3p$ band, the corresponding $3p$ bandwidth is larger by at least 0.5 eV compared with the $4p$

bandwidth of the Ga clusters. This is in contrast to the spectra of the smaller clusters which exhibit approximately equal bandwidths of the 3*p* and 4*p* bands.

A possible reason for this behavior might be the onset of hybridization of the 3*s* and 3*p* bands. In the spectra of the smaller Al_n^- clusters ($n<8$), a feature observed at high BE was assigned to the antibonding orbital of the 3*s* derived states. However, in the case of Al_6^- and Al_7^-, this assignment is rather uncertain. With increasing cluster size, the gap between the two bands is expected to decrease. Thus, if the assignment of feature *D* in the spectra of Al_6^- and Al_7^- is correct, the difference in BE between the antibonding 3*s* orbital and the lowest 3*p* derived states is about 0.5 eV in these clusters. From a comparison of Cu_n^- and Ag_n^- spectra, we found a clear indication of *s–d* hybridization for Cu_n^- at about 0.5 eV difference in BE.[16] From these considerations, an onset of hybridization between the antibonding 3*s* and the 3*p* orbitals is expected beyond $n=8$, in agreement with the observed increase in the 3*p* bandwidth. However, a clear picture can only be gained from spectra taken at higher photon energy[38] and from supporting calculations.

The spectra of the Ga_n^- clusters with $n=8$–11 (Fig. 5) vary only slightly compared with the spectra of the larger and smaller Ga clusters. All observed features are assigned to photodetachment from 4*p* derived molecular orbitals. The bandwidth does not change drastically and the number of resolved peaks varies between three and five. This supports the assumption of an onset of *s–p* hybridization for the Al clusters of the same size. The hybridization is accompanied by an increase of the *p* bandwidth not observed for Ga clusters of the same size. In Ga, the *s* band has a higher BE and therefore the onset of hybridization is shifted towards larger cluster sizes.

8. Al_n^-/Ga_n^-, $n=12$–15

Again the pattern observed in the spectra of the larger Al clusters changes dramatically compared with the size regime $n=8$–11. The spectra of Al_{12}^-–Al_{15}^- (Fig. 4) simplify and a single feature *A* located at 3.5–4.0 eV BE dominates the photodetachment signal. Except for Al_{13}^-, this single feature is accompanied by one or two additional peaks (marked *B* and *C*) at lower BE.

Al_{13}^- displays only a single relatively narrow feature (Fig. 4). This high degeneracy of the electronic states corresponds to a pronounced maximum of the size dependence of the VDE (see below). The high VDE of this cluster can be explained by a shell closing corresponding to 40 electrons in terms of the jellium model. However, our photoelectron data of the small clusters do not support the jellium picture for these particles and therefore the observations for Al_{13}^- have to be explained using more complex models. Quantum chemical calculations[10] predict a highly symmetric icosahedral geometric structure for the Al_{13}^- anion. This cluster is therefore very similar to a neutral rare gas cluster of 13 atoms and approaches a spherical geometry as closely as possible. Due to the high geometrical symmetry, the electron orbitals are highly degenerate in agreement with the photoelectron spectrum. We assign peak *A* in the spectrum of Al_{13}^- to photodetachment from molecular orbitals derived from the 3*p* states of the atoms. However, as discussed for the smaller Al clusters, we cannot exclude a contribution from 3*s* derived orbitals.

The spectrum of Ga_{13}^- exhibits a double peak (Fig. 5, marked *A*) which might be due to a reduced symmetry compared with Al_{13}^- or the "general" difference in the *s–p* hybridization. However, there is still a pronounced maximum of the VDE for $n=13$ and the 4*p* bandwidth has a minimum indicating an increased degeneracy of states for Ga_{13}^-. Therefore, Ga_{13}^- can be assigned to a "magic number" cluster, but the structural symmetry could possibly be lower than in Al_{13}^-.

Based on the assignment of feature *A* of the spectra of Al_{12}^-–Al_{15}^-, the additional features observed in the spectrum of Al_{12}^-, Al_{14}^-, and Al_{15}^- can be understood qualitatively. For Al_{12}^-, the spherical symmetry is not quite achieved and the 3*p* derived orbitals are not completely degenerate. The spectrum of Al_{14}^- is very similar to the one of Al_{12}^-. This might be due to the fact that either one differs from the magic number cluster by one atom. The splitting of the partially degenerate 3*p* orbitals is similar if there is a hole in the icosahedral shell, or if an additional atom "sits" on the icosahedron. The spectrum of Al_{15}^- displays only a single additional peak with a slightly increased intensity compared with one of the corresponding features observed for Al_{14}^-. Its BE is about the average BE between the two Al_{14}^- peaks. This observation should again be related to the geometric structure of the cluster, but high level calculations are necessary to gain a reliable assignment.

The pattern observed in the spectra of Al_{12}^-–Al_{15}^- can also be identified for Ga_{12}^-–Ga_{15}^-. For Ga_{12}^-–Ga_{14}^-, the prominent feature *A* observed in the Al spectra is split into a double peak. We observe analogous additional peaks as for Al. In the case of Ga_{15}^-, the prominent feature even seems to be split into three peaks, but due to the decreased signal to noise ratio in this spectrum, the splitting is difficult to establish. The discussion of the small additional features is analogous to the Al data. The discussion of the spectra of Ga_{12}^-–Ga_{15}^- in terms of the observation of a split main feature and some additional features at low BE is based on the observation of this pattern for the Al clusters of the same size. We note that this pattern is not obvious without the prior knowledge of the Al data.

VI. ELECTRON AFFINITIES

The electron affinity (E.A.) is commonly defined as the energy gained if an additional electron is added to the neutral cluster. Analogous to the case of the ionization potentials of neutrals, one has to distinguish between a vertical E.A. and an adiabatic E.A. The adiabatic E.A. is the difference in binding energy between the two electronic ground states in their relaxed geometry. The vertical E.A. is the difference in binding energy between the neutral ground state and the electronic ground state of the anion with the nuclei fixed at the positions corresponding to the neutral ground state geometry. This usually corresponds to a vibrationally excited state of the anion and is described

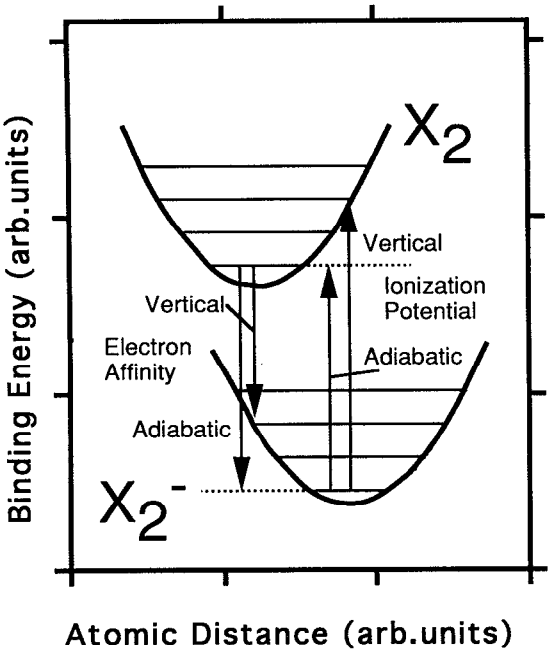

FIG. 8. An illustration of the differences between the electron affinity (E.A.) of the neutral cluster and the ionization potential of the anion. The figure displays the schematic potential curves of the ground states of a neutral (X_2) and a negatively charged dimer (X_2^-). The lowest vibrational levels are also displayed in the figure. The equilibrium distances of the two charge states of the dimer are different. The adiabatic E.A. corresponds to the transition from the vibrational ground state of the neutral into the vibronic ground state of the anion. The adiabatic ionization potential corresponds to the inverse process and is equal to the adiabatic E.A. The vertical ionization potential (VDE=vertical electron detachment energy) corresponds to the transition from the vibronic ground state of the anion into a vibrationally excited state of the neutral. The coordinates of the nuclei are fixed during the transition. A photodetachment experiment measures the VDE, except for cases when the 0–0 vibrational transition can be identified in the spectrum.

by the Franck–Condon principle. If the ground state geometries differ, the vertical E.A. is smaller than the adiabatic E.A.

However, with our experimental method, we determine the vertical ionization potential of the anion (VDE[28] =vertical electron detachment energy), which differs from the vertical and the adiabatic E.A. Figure 8 illustrates the different transitions connected to the different quantities. The adiabatic ionization potential of the anion corresponds to the transition from the anion ground state into the neutral ground state. The adiabatic ionization potential of the anion is equal to the adiabatic electron affinity of the neutral cluster. The VDE corresponds to the transition from the ground state of the anion into the neutral electronic ground state with the nuclei frozen in the anion ground state geometry. This energy is measured by a photodetachment experiment because the removal of the electron is a fast process compared with the movement of the nuclei. The VDE is in most cases larger than the adiabatic electron affinity. Only if the vibrational structure of the electronic ground state transition is resolved and the 0–0 vibrational transition is identified the adiabatic electron affinity can be determined.[27,28]

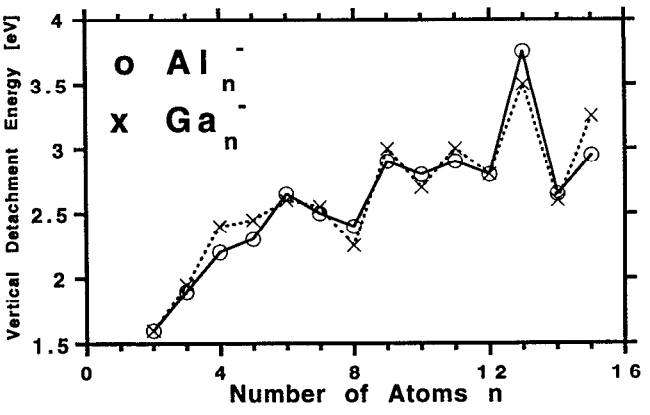

FIG. 9. The VDE (see the text for definition) of the Al and Ga clusters extracted from the photoelectron spectra obtained using 3.68 eV laser radiation. The value is determined as the peak position of the feature at lowest BE assigned to the bare cluster. Starting from $n=7$, a weak even–odd alternation is observed. The amplitude of the alternation increases with a local maximum at $n=13$. The uncertainty of the absolute binding energy is ± 0.1 eV. The determination of the size dependent relative shifts of the VDEs between two clusters is more accurate (± 10–20 meV). The resulting error of the displayed values corresponds to about the size of the symbols (× and ○).

Figure 9 displays the VDEs of Al_n^- and Ga_n^- extracted from the photoelectron spectra taken at $h\nu=3.68$ eV. The values are also listed in Table I. The VDE is determined as the center of the peak at lowest BE. The VDEs are expected to exhibit an even–odd alternation for metals with an odd number of valence electrons per atom. The data displayed in Fig. 9 do not exhibit a pronounced alternation for smaller Al clusters ($n<7$). Starting at $n=7$, a weak alternation is observed. The amplitude of the alternation is largest at $n=13$. However, due to the limited set of data, it is uncertain if the alternation continues to larger clusters. Earlier measurements[21] on Al_n^- clusters did not show an alternation, which might be due to the limited energy resolution in these experiments. A similar behavior is found for Ga_n^- (Fig. 9). The amplitude of the even–odd alterna-

TABLE I. Vertical electron detachment energies (VDEs) as determined from the electron spectra. The absolute error of the energies is ±0.1 eV.

Number of atoms n	Aluminum (eV)	Gallium (eV)
2	1.60	1.60
3	1.90	1.95
4	2.20	2.40
5	2.30	2.45
6	2.65	2.60
7	2.50	2.55
8	2.40	2.25
9	2.90	3.00
10	2.80	2.70
11	2.90	3.00
12	2.80	2.80
13	3.75	3.50
14	2.65	2.60
15	2.95	3.25

tion is comparable to Al_n^-, but for both metals, the alternations are much weaker in amplitude than those observed for the coinage metal or alkali clusters of the same size.[14]

The lack of an odd–even alternation for the small clusters ($n<7$) is in disagreement with the predictions of the ellisoidal JM.[14] These very small clusters are not spherical and the electronic shells split into single electron orbitals. Thus, each orbital corresponds to a subshell and shell closings occur for all even numbers of electrons. Even if the electrons occupy localized but nondegenerate orbitals, an alternation should be observed. There are two possible explanations for the lack of an alternation: (1) there are highly degenerate molecular orbitals arising from a high symmetry; or (2) the electron–electron interaction changes the occupation of nondegenerate orbitals preferring higher spin multiplicities. For the very small planar clusters, there are σ and π orbitals (see above). These orbitals are very close in BE, but usually not perfectly degenerate. However, the density of valence electrons confined in the cluster is three times higher compared with alkali clusters. Therefore the electron–electron interaction is strong and the occupation of the nearly degenerate σ and π orbitals may differ from the singlet–doublet scheme observed for monovalent metal clusters preferring high spin states. This behavior is predicted[10] for neutral Al clusters with $n<6$.

This also explains the appearance of a weak alternation for the larger clusters (Fig. 9). The increasing diameter of the electron orbitals for larger clusters causes a decrease in interaction energy between electrons in delocalized orbitals. With increasing cluster size, the electrons tend to occupy the orbitals depending on the BE only. The appearance of an even–odd alternation is expected and the ground states of the clusters alternate between singlet and doublet states.

The maximum of the VDE at $n=13$ can be explained by the high symmetry of the icosahedral Al_{13}^- indicated by the observation of one narrow feature in the photoelectron spectrum (Fig. 4) only. The high anion symmetry is due to a coincidence of geometrical and electronic shell closings occurring at 13 atoms and 40 electrons.

The onset of the even–odd alternation at $n=7$ coincides roughly with the observed change in the structure of the photoelectron spectra at $n=8$. The spectra support the assumption of a planar symmetry for the very small Al_n^- clusters up to $n=5$. Beyond $n=7$, the photoelectron spectra exhibit a congestion of peaks, which simplifies around $n=13$. The change of the pattern observed in the spectra might by caused by the transition from a planar symmetry to a spherical symmetry. Al_5^- is planar (or close to planar) and Al_{13}^- exhibits an icosahedral symmetry[10] close to that of a sphere. The transition from 2D to 3D takes place in between. The spectra of Al_6^- and Al_7^- exhibit some resemblances with Al_5^- indicating a similarity of structure.

The onset of the even–odd alternation coincides with the onset of the transition from 2D to 3D structure. The small planar clusters exhibit nearly degenerate molecular orbitals with σ and π symmetries, and calculations[10] predict that states with high spin multiplicities are more stable than minimum spin states. Starting from $n=5$, the clusters gradually prefer 3D structures. The splitting of the close lying orbitals increases beyond $n=7$ and the electron–electron interaction decreases due to the increased distance between delocalized electrons. Accordingly, the ground states are either singlet or doublet states and an even–odd alternation is observed.

VII. SUMMARY

We have presented photoelectron spectra of Al_n^- and Ga_n^- clusters taken at two different photon energies ($h\nu = 3.68$ and 5.0 eV). The energy resolution (30–100 meV) of the photoelectron spectrometer is sufficient to resolve much more details than earlier measurements.[21–23]

The photoelectron spectra have been compared qualitatively with the results of quantum chemical calculations.[1–10] The spectra can be divided into three size regimes which correspond to the predicted transition from a planar to a compact 3D structure of the particles.

A. $n=2$–7

The clusters with $n=2$–5 are predicted to be planar. The features observed at low BEs for $n=2$–4 are assigned to σ and π orbitals in agreement with the calculations. For Al_n^-, a feature observed at higher BE is assigned to the antibonding orbital of the 3*s* band. The 4*s* band of Ga is located at about 1 eV higher BE. The features corresponding to 3*p*/4*p* derived orbitals in the spectra of Al and Ga clusters are very similar. The spectrum of Al_5^- resembles the same pattern as the spectrum of Al_4^- supporting the assumption of a planar structure of the pentamer. For $n=6$ and 7, the spectra still exhibit a certain similarity to the spectra of the smaller clusters, which might correspond to a nearly planar or buckled geometry of these particles.

B. $n=8$–11

The bandwidth of the 3*p* derived orbitals increases gradually with cluster size. The spectra of Al_n^- with $n=8$–11 exhibit an increasing number of partially overlapping features. We suppose this increasing complexity corresponds to the transition from a planar to a 3D structure. Within this transition region, the symmetry of the clusters is rather low. The similarity to the spectra of Ga_n^- clusters decreases gradually with *n*, which can be explained by the onset of hybridization of the Al 3*p* orbitals with the antibonding 3*s* derived orbital. The hybridization occurs in Ga at higher *n* due to the larger *s*–*p* gap and is beyond the size range of our present work.

C. $n=12$–15

The structure of the spectra of Al_n^- simplifies again and only a few peaks are observed. The single feature observed in the spectrum of Al_{13}^- is in qualitative agreement with the predicted high symmetry of the icosahedral particle.[4] The spectra of Al_{12}^- and Al_{15}^- are similar and exhibit one main feature and two smaller peaks at low BE. This splitting might correspond to a reduced symmetry of these particles. The reduction in symmetry is similar for an ad-

ditional atom or the lack of one atom with respect to the 13 atom icosahedra. In general, the spectra of Al_n^- with $n=11$–15 are similar and therefore we propose a geometric structure close to a sphere for these particles. The spectra of Ga_n^- exhibit a certain similarity to the Al spectra. However, the main feature is split into two or three peaks.

The spectra of the clusters with $n<12$ show no similarities to an electronic shell structure observed for monovalent clusters. From the comparison with quantum chemical calculations, the development of a shell can be expected when the s and p bands start to merge. We find hints for the onset of s–p hybridization for Al_n^- beyond $n=7$. For the test of the validity of the JM, data taken at higher photon energies and extended to larger cluster sizes are necessary.[38]

ACKNOWLEDGMENTS

We thank Jürger Lauer and Heinz Pfeifer for their technical support. Paul Bechthold and Haiko Handschuh helped with experimental problems and the understanding of the data. The most important impact on our work came from Robert O. Jones with his suggestion to compare Ga to the Al data and with lively discussions when visiting the laboratory.

[1] R. O. Jones, Phys. Rev. Lett. **67**, 224 (1991).
[2] T. H. Upton, Phys. Rev. Lett. **56**, 2168 (1986).
[3] U. Meier, S. D. Peyerimhoff, and F. Grein, Z. Phys. D **17**, 209 (1990).
[4] U. Röthlisberger, W. Andreoni, and P. Giannozzi, J. Chem. Phys. **96**, 1248 (1992).
[5] H. Basch, Chem. Phys. Lett. **136**, 289 (1987).
[6] L. G. M. Petterson, C. W. Bauschlicher, and T. Halicioglu, J. Chem. Phys. **87**, 2205 (1987).
[7] J. Koutecky, G. Paccioni, G. H. Jeung, and E. C. Hass, Surf. Sci. **156**, 650 (1985).
[8] T. Bastug, W. D. Sepp, B. Fricke, D. Heinemann, and D. Kolb, Z. Phys. D **22**, 641 (1992).
[9] R. O. Jones, Z. Phys. D **26**, 23 (1993).
[10] R. O. Jones, J. Chem. Phys. **99**, 1194 (1993).
[11] T. P. Martin, T. Bergmann, H. Göhlich, and T. Lange, Chem. Phys. Lett. **176**, 343 (1991).
[12] W. D. Knight, K. Clemenger, W. A. de Heer, W. A. Saunders, M. Y. Chou, and M. L. Cohen, Phys. Rev. Lett. **24**, 2141 (1984).
[13] W. Ekardt, and Z. Penzar, Phys. Rev. B **38**, 4273 (1988).
[14] W. A. de Heer, Rev. Mod. Phys. **65**, 611 (1993).
[15] C.-Y. Cha, G. Ganteför, and W. Eberhardt, Z. Phys. D **26**, 307 (1993).
[16] C.-Y. Cha, G. Ganteför, and W. Eberhardt, J. Chem. Phys. **99**, 6308 (1993).
[17] See, e.g., W. A. Harrison, *Electronic Structure and the Properties of Solids* (Freeman, San Francisco, 1980).
[18] W. A. de Heer, P. Milani, and A. Chatelain, Phys. Rev. Lett. **63**, 2834 (1989).
[19] K. E. Schriver, J. L. Persson, E. C. Honea, and R. L. Whetten, Phys. Rev. Lett. **64**, 2539 (1990).
[20] C.-Y. Cha, G. Ganteför, and W. Eberhardt, Rev. Sci. Instrum. **63**, 5661 (1992).
[21] K. J. Taylor, C. L. Pettiette, M. J. Craycraft, O. Chesnovsky, and R. E. Smalley, Chem. Phys. Lett. **152**, 347 (1988).
[22] G. Ganteför, K. H. Meiwes-Broer, and H. O. Lutz, Phys. Rev. A **37**, 2716 (1988).
[23] G. Ganteför, M. Gausa, K. H. Meiwes-Broer, and H. O. Lutz, Z. Phys. D **9**, 253 (1988).
[24] G. Ganteför, H. R. Siekmann, H. O. Lutz, and K.-H. Meiwes-Broer, Chem. Phys. Lett. **165**, 293 (1990).
[25] H. R. Siekmann, C. Lüder, J. Faehrmann, H. O. Lutz, and K. H. Meiwes-Broer, Z. Phys. D **20**, 417 (1991).
[26] G. F. Gantefor, D. M. Cox, and A. Kaldor, J. Chem. Phys. **93**, 8395 (1990).
[27] K. M. Ervin and W. C. Lineberger, Adv. Gas Phase Ion Chem. **1**, 121 (1992).
[28] J. Hoe, K. M. Ervin, and W. C. Lineberger, J. Chem. Phys. **93**, 6987 (1990).
[29] See, e.g., C. R. C. Wang, S. Pollack, D. Cameron, and M. M. Kappes, J. Chem. Phys. **93**, 3787 (1990).
[30] K. Selby, M. Vollmer, J. Masui, V. Kresin, W. A. de Heer, and W. D. Knight, Phys. Rev. B **40**, 5417 (1989).
[31] T. H. Upton, J. Chem. Phys. **86**, 7054 (1987).
[32] H. Hotop, and W. C. Lineberger, J. Phys. Chem. Ref. Data **14**, 731 (1985).
[33] C. F. Moore, Natl. Bur. Stand., Ref. Data Ser. **35**, xxx (1971).
[34] E. P. Wigner, Phys. Rev. **73**, 1002 (1948).
[35] See, e.g., G. F. Ganteför, D. M. Cox, and A. Kaldor, J. Chem. Phys. **96**, 4102 (1992).
[36] G. F. Ganteför, D. M. Cox, and A. Kaldor (unpublished results).
[37] For example, Ag_{13}^- from G. Ganteför, M. Gausa, K. H. Meiwes-Broer, and H. O. Lutz, Faraday Discuss. Chem. Soc. **86**, 197 (1988).
[38] G. Ganteför and W. Eberhardt (to be published).
[39] K. M. McHugh, J. G. Eaton, G. H. Lee, H. W. Sarkas, L. H. Kidder, J. T. Snodgrass, M. R. Manaa, and K. H. Bowen, J. Chem. Phys. **91**, 3792 (1989).
[40] M. F. Cai, T. P. Djugan, and V. E. Bondybey, Chem. Phys. Lett. **155**, 430 (1989).
[41] T. N. Kitsopoulos, C. J. Chick, Z. Zhao, and D. M. Neumark, J. Chem. Phys. **95**, 1441 (1991).